

基于损耗和高斯噪声的连续变量 多组分 EPR 导引操控

翟淑琴^{1,2*}, 袁楠¹

¹ 山西大学物理电子工程学院, 山西 太原 030006;

² 山西大学光电子研究所量子光学与光量子器件国家重点实验室, 太原 030006

摘要 多组分 EPR 导引可以通过操控不同量子节点中的信息来实现安全量子网络,是安全量子网络的核心资源。通过在连续变量光场中加入分束器模拟损耗和高斯噪声的方式实现了多组分 EPR 导引。通过建立多组分纠缠态间的协方差矩阵,量化了纠缠态间的 EPR 导引特性。此外,研究了 EPR 导引参数随高斯噪声及分束器透射率的变化关系,实现了不同模式间的单向 EPR 导引,为实现安全量子通信的单向性提供了参考。

关键词 量子光学; EPR 导引; 单向导引; 不对称性; 噪声; 量子网络

中图分类号 O437 文献标志码 A

doi: 10.3788/CJL202148.2012001

1 引言

Einstein 等^[1]为证明量子力学的不完备性,提出了 EPR 佯谬。随后, Schrödinger^[2]提出“导引”一词来描述 EPR 佯谬中的“幽灵般的超距作用”,在此基础上, Wiseman 等^[3]正式定义了 EPR 导引。EPR 导引是一种特殊的量子关联,描述了测量一个粒子非局域地影响另一个粒子状态的能力。假设 Alice 和 Bob 共享一个空间上分离的 EPR 纠缠态, EPR 导引是指 Alice 可以通过执行测量来导引 Bob 的状态,或者 Bob 可以通过执行测量来导引 Alice 的状态。Alice 可以导引 Bob,但是 Bob 无法导引 Alice,或者 Bob 可以导引 Alice,但是 Alice 无法导引 Bob,均是单向 EPR 导引^[3]。正是由于这种特殊的不对称性质, EPR 导引可应用于单端量子通信领域,如单端设备无关的量子密钥分发^[4-7]、量子秘密共享^[8]、安全量子隐形传态^[9-11]以及安全量子网络^[12-14]。

2012 年, Händchen 等^[15]利用高斯纠缠态来验证连续变量不对称量子导引,推动量子安全通信领域的发展进入了新阶段。之后, He 等^[16]将量子导

引从连续变量两组分系统扩展到多组分系统,并提出了真正的三组分导引概念。此外,他们还对光量子网络中存在多组分 EPR 导引和真正的三组分纠缠进行了实验验证^[17]。2017 年, Qin 等^[18]通过在量子网络中加入热噪声或改变量子通道中透射率的方式实现了量子系统的不对称性。特别是,利用多组分纠缠可以实现单向量子计算^[19-20]。2014 年, Bowles 等^[21]实现了两量子比特纠缠态的单向量子导引。同年, Skrzypczyk^[22]用一个任意集合的正值测量证实了单向量子导引的导引特性。之后,研究人员们提出了一些更为实用的方法,如通过协方差矩阵来量化纠缠态之间的非对称 EPR 导引^[23]。

由于连续变量 Cluster 纠缠态^[24-25]比 GHZ 态具有更好的纠缠稳定性^[26],故与基于 GHZ 态的多组分子子导引方案^[27-28]相比,利用基于 Cluster 纠缠态的多组分子子导引方案更容易实现量子通信的操控^[29-30]。因此,基于连续变量 Cluster 纠缠态的量子导引^[31]及其应用价值仍值得进一步探索。

2019 年,我们通过对四组分方形 Cluster 纠缠态进行非对称调制,实现了四组分到三组分及三组分到

收稿日期: 2021-01-25; 修回日期: 2021-02-10; 录用日期: 2021-03-15

基金项目: 国家自然科学基金(12074233, 91536222, 11674205)、国家 973 计划(2016YFA0301404)、山西省自然科学基金(201801D121121)、2017 年山西省高等学校教学改革创新项目(J2017006)

通信作者: *xiaozhai@sxu.edu.cn

两组分不同模式组合间的 EPR 导引^[32]。随后,又研究了引入噪声后的两组分 EPR 导引和非对称调制后的两组分 EPR 导引间的区别^[33]。本文基于四组分方形 Cluster 纠缠态,研究了两组分、三组分、四组分间的量子导引特性。通过加入适量的高斯噪声以及调节分束器透射率,研究了可在大范围内实现单向 EPR 导引的途径。该研究结果对于量子安全通信^[34]、量子离物传态、量子秘密共享方案以及单端设备无关的量子密钥分发等领域具有重要意义。

2 物理模型

图 1 为多组分 EPR 导引方向操控的示意图。此方案由两对振幅压缩模和两对相位压缩模先后通过透射率分别为 T_1 、 T_2 、 T_3 的三个分束器 (BS_1 、 BS_2 、 BS_3) 进行耦合。图 1 中 ‘i’ 和 ‘-1’ 分别表示光模在相位空间内进行了 90° 和 180° 的翻转, \hat{A} 、 \hat{B} 、 \hat{C} 、 \hat{D} 为四个输出模。 \hat{A} 端远程传输时具有一定的损耗,用分束器模型引入损耗信道后 \hat{A} 变为 \hat{A}' , \hat{B} 端通过一个 99:1 的分束器 BS_4 耦合入高斯噪声算符 $\hat{\delta}$ 后变为 \hat{B}' 。最终,可利用 4 个零拍探测器 (HD_1 、 HD_2 、 HD_3 、 HD_4) 来探测 4 个输出模的结果。

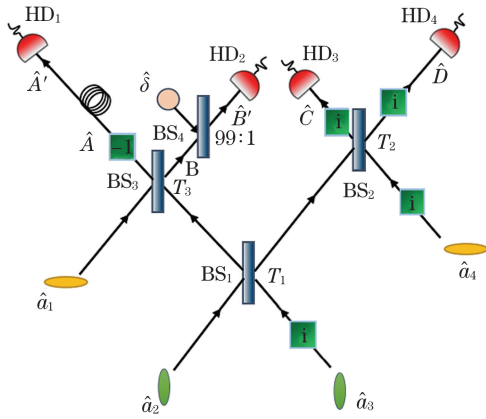


图 1 多组分 EPR 导引方向操控示意图

Fig. 1 Schematic diagram of manipulating direction of multipartite EPR steering

\hat{a}_1 和 \hat{a}_4 是相位压缩模, \hat{a}_2 和 \hat{a}_3 是振幅压缩模, 四个初始输入模的表达式为

$$\begin{cases} \hat{a}_1 = \frac{1}{2} [\exp(r_1)\hat{X}_1^{(0)} + i\exp(-r_1)\hat{P}_1^{(0)}] \\ \hat{a}_2 = \frac{1}{2} [\exp(-r_2)\hat{X}_2^{(0)} + i\exp(r_2)\hat{P}_2^{(0)}] \\ \hat{a}_3 = \frac{1}{2} [\exp(-r_3)\hat{X}_3^{(0)} + i\exp(r_3)\hat{P}_3^{(0)}] \\ \hat{a}_4 = \frac{1}{2} [\exp(r_4)\hat{X}_4^{(0)} + i\exp(-r_4)\hat{P}_4^{(0)}] \end{cases}, \quad (1)$$

式中: $\hat{X}_j = \hat{a}_j + \hat{a}_j^\dagger$ 和 $\hat{P}_j = (\hat{a}_j - \hat{a}_j^\dagger)/i$ ($j=1, 2, 3, 4$) 分别表示光模 \hat{a}_j 的正交振幅算符和正交相位算符; $\hat{X}^{(0)}$ 和 $\hat{P}^{(0)}$ 表示真空模的正交振幅算符和正交相位算符。 $r_1=r_2=r_3=r_4$ 表示光模的压缩参数。将 4 个初始输入模耦合进三个透射率分别为 $T_1=0.2$ 、 $T_2=T_3=0.5$ 的分束器中, 4 个输出模的表达式为

$$\begin{cases} \hat{A} = -\sqrt{\frac{1}{2}}\hat{a}_1 - \sqrt{\frac{2}{5}}\hat{a}_2 - i\sqrt{\frac{1}{10}}\hat{a}_3 \\ \hat{B} = \sqrt{\frac{1}{2}}\hat{a}_1 - \sqrt{\frac{2}{5}}\hat{a}_2 - i\sqrt{\frac{1}{10}}\hat{a}_3 \\ \hat{C} = i\sqrt{\frac{1}{10}}\hat{a}_2 + \sqrt{\frac{2}{5}}\hat{a}_3 - \sqrt{\frac{1}{2}}\hat{a}_4 \\ \hat{D} = i\sqrt{\frac{1}{10}}\hat{a}_2 + \sqrt{\frac{2}{5}}\hat{a}_3 + \sqrt{\frac{1}{2}}\hat{a}_4 \end{cases}. \quad (2)$$

在图 1 中, 模 \hat{A} 通过由分束器模型引入的量子损耗信道后, 输出模为 \hat{A}' , 其表达式为

$$\hat{A}' = \sqrt{\eta}\hat{A} + \sqrt{1-\eta}\hat{\nu}, \quad (3)$$

式中: η 表示量子损耗信道中的透射率; $\hat{\nu}$ 表示真空模。模 \hat{B} 通过一个 99:1 的分束器, 耦合入高斯噪声算符 $\hat{\delta}$ 后, 其输出模 \hat{B}' 的表达式为 $\hat{B}' = \hat{B} + \hat{\delta}$ 。

4 个输出模的正交振幅算符和正交相位算符的表达式为

$$\begin{cases} \hat{X}_{A'} = \sqrt{\eta} [\text{Re}(-\sqrt{\frac{1}{2}}\hat{a}_1 - \sqrt{\frac{2}{5}}\hat{a}_2) + \text{Im}(\sqrt{\frac{1}{10}}\hat{a}_3)] + \sqrt{1-\eta}\hat{X}_\nu \\ \hat{P}_{A'} = \sqrt{\eta} [\text{Im}(-\sqrt{\frac{1}{2}}\hat{a}_1 - \sqrt{\frac{2}{5}}\hat{a}_2) - \text{Re}(\sqrt{\frac{1}{10}}\hat{a}_3)] + \sqrt{1-\eta}\hat{P}_\nu \\ \hat{X}_{B'} = \text{Re}(\sqrt{\frac{1}{2}}\hat{a}_1 - \sqrt{\frac{2}{5}}\hat{a}_2) + \text{Im}(\sqrt{\frac{1}{10}}\hat{a}_3) + \hat{X}_\delta \\ \hat{P}_{B'} = \text{Im}(\sqrt{\frac{1}{2}}\hat{a}_1 - \sqrt{\frac{2}{5}}\hat{a}_2) - \text{Re}(\sqrt{\frac{1}{10}}\hat{a}_3) + \hat{P}_\delta \\ \hat{X}_C = -\text{Im}(\sqrt{\frac{1}{10}}\hat{a}_2) + \text{Re}(\sqrt{\frac{2}{5}}\hat{a}_3 - \sqrt{\frac{1}{2}}\hat{a}_4) \\ \hat{P}_C = \text{Re}(\sqrt{\frac{1}{10}}\hat{a}_2) + \text{Im}(\sqrt{\frac{2}{5}}\hat{a}_3 - \sqrt{\frac{1}{2}}\hat{a}_4) \\ \hat{X}_D = -\text{Im}(\sqrt{\frac{1}{10}}\hat{a}_2) + \text{Re}(\sqrt{\frac{2}{5}}\hat{a}_3 + \sqrt{\frac{1}{2}}\hat{a}_4) \\ \hat{P}_D = \text{Re}(\sqrt{\frac{1}{10}}\hat{a}_2) + \text{Im}(\sqrt{\frac{2}{5}}\hat{a}_3 + \sqrt{\frac{1}{2}}\hat{a}_4) \end{cases}, \quad (4)$$

式中： \hat{X}_ν 和 \hat{P}_ν 分别表示由分束器引入的真真空态 $\hat{\nu}$ 的正交振幅算符和正交相位算符； \hat{X}_δ 和 \hat{P}_δ 分别表示所加高斯噪声算符 $\hat{\delta}$ 的正交振幅算符和正交相位算符。

为研究系统中不同模式之间的导引特性，假设两个多组分纠缠态系统分别为 A 和 B ， n_A 和 m_B 分别表示子系统 A 中包含 n 个光学模，子系统 B 中包含 m 个光学模，其中 $n=1,2,3, m=1,2,3$ 。则这个系统($n_A + m_B$)的导引特性可以用它的协方差矩阵^[35-36]来确定，其形式为

$$\sigma_{AB} = \begin{pmatrix} \mathbf{A} & \mathbf{C} \\ \mathbf{C}^T & \mathbf{B} \end{pmatrix}, \quad (5)$$

式中：子矩阵 \mathbf{A} 和 \mathbf{B} 分别表示子系统 A 和子系统 B 的协方差矩阵； \mathbf{C} 表示 \mathbf{A} 和 \mathbf{B} 两个子矩阵的交叉矩阵。在矩阵元 $\sigma_{ij} = \langle \hat{\xi}_i \hat{\xi}_j + \hat{\xi}_j \hat{\xi}_i \rangle / 2 - \langle \hat{\xi}_i \rangle \langle \hat{\xi}_j \rangle$ 中， $\hat{\xi}$ 为光学场的正交算符，包括正交振幅 $\hat{X} = a + a^\dagger$ 和正交相位 $\hat{P} = (a - a^\dagger) / i$ ， $\hat{\xi} \equiv (\hat{X}_1^A, \hat{P}_1^A, \dots, \hat{X}_n^A, \hat{P}_n^A, \hat{X}_1^B, \hat{P}_1^B, \dots, \hat{X}_m^B, \hat{P}_m^B)$ 。

\hat{A}' 模和 \hat{B}' 模的两组分系统的导引特性由协方差矩阵确定：

$$\sigma_{11} = \begin{bmatrix} \sigma_{A'A'} & \sigma_{A'B'} \\ \sigma_{A'B'}^T & \sigma_{B'B'} \end{bmatrix}, \quad (6)$$

式中：子矩阵的表达式为

$$\left\{ \begin{array}{l} \sigma_{A'A'} = \begin{bmatrix} \text{Cov}(\hat{X}_{A'}, \hat{X}_{A'}) & \text{Cov}(\hat{X}_{A'}, \hat{P}_{A'}) \\ \text{Cov}(\hat{P}_{A'}, \hat{X}_{A'}) & \text{Cov}(\hat{P}_{A'}, \hat{P}_{A'}) \end{bmatrix} \\ \sigma_{B'B'} = \begin{bmatrix} \text{Cov}(\hat{X}_{B'}, \hat{X}_{B'}) & \text{Cov}(\hat{X}_{B'}, \hat{P}_{B'}) \\ \text{Cov}(\hat{P}_{B'}, \hat{X}_{B'}) & \text{Cov}(\hat{P}_{B'}, \hat{P}_{B'}) \end{bmatrix} \\ \sigma_{A'B'} = \begin{bmatrix} \text{Cov}(\hat{X}_{A'}, \hat{X}_{B'}) & \text{Cov}(\hat{X}_{A'}, \hat{P}_{B'}) \\ \text{Cov}(\hat{P}_{A'}, \hat{X}_{B'}) & \text{Cov}(\hat{P}_{A'}, \hat{P}_{B'}) \end{bmatrix} \\ \sigma_{A'B'}^T = \begin{bmatrix} \text{Cov}(\hat{X}_{A'}, \hat{X}_{B'}) & \text{Cov}(\hat{P}_{A'}, \hat{X}_{B'}) \\ \text{Cov}(\hat{X}_{A'}, \hat{P}_{B'}) & \text{Cov}(\hat{P}_{A'}, \hat{P}_{B'}) \end{bmatrix} \end{array} \right., \quad (7)$$

将(4)式代入子矩阵的矩阵元中，可得

$$\left\{ \begin{array}{l} \text{Cov}(\hat{X}_{A'}, \hat{X}_{A'}) = \Delta^2 \hat{X}_{A'} = \eta \left[\frac{3}{5} \exp(2r) + \frac{2}{5} \exp(-2r) \right] + (1 - \eta) \Delta^2 (\hat{X}_\nu) \\ \text{Cov}(\hat{P}_{A'}, \hat{P}_{A'}) = \Delta^2 \hat{P}_{A'} = \eta \left[\frac{3}{5} \exp(-2r) + \frac{2}{5} \exp(2r) \right] + (1 - \eta) \Delta^2 (\hat{P}_\nu) \\ \text{Cov}(\hat{X}_{B'}, \hat{X}_{B'}) = \Delta^2 \hat{X}_{B'} = \frac{3}{5} \exp(2r) + \frac{2}{5} \exp(-2r) + \Delta^2 (\hat{X}_\delta) \\ \text{Cov}(\hat{P}_{B'}, \hat{P}_{B'}) = \Delta^2 \hat{P}_{B'} = \frac{3}{5} \exp(-2r) + \frac{2}{5} \exp(2r) + \Delta^2 (\hat{P}_\delta) \\ \text{Cov}(\hat{X}_{A'}, \hat{X}_{B'}) = \sqrt{\eta} \left[-\frac{2}{5} \exp(2r) + \frac{2}{5} \exp(-2r) \right] \\ \text{Cov}(\hat{P}_{A'}, \hat{P}_{B'}) = \sqrt{\eta} \left[-\frac{2}{5} \exp(-2r) + \frac{2}{5} \exp(2r) \right] \\ \text{Cov}(\hat{X}_{A'}, \hat{P}_{A'}) = \text{Cov}(\hat{P}_{A'}, \hat{X}_{A'}) = \text{Cov}(\hat{X}_{B'}, \hat{P}_{B'}) = \text{Cov}(\hat{P}_{B'}, \hat{X}_{B'}) = \\ \text{Cov}(\hat{X}_{A'}, \hat{P}_{B'}) = \text{Cov}(\hat{P}_{A'}, \hat{X}_{B'}) = \text{Cov}(\hat{P}_{A'}, \hat{X}_{B'}) = \text{Cov}(\hat{X}_{A'}, \hat{P}_{B'}) = 0 \end{array} \right., \quad (8)$$

式中： $\Delta^2 (\hat{X}_\delta) = \Delta^2 (\hat{P}_\delta) = \delta$ ； $\Delta^2 (\hat{X}_\nu) = \Delta^2 (\hat{P}_\nu) = 1$ ； $\text{Cov}(\cdot)$ 为协方差函数。

三个模式的协方差矩阵为

$$\sigma_{12} = \sigma_{21} = \begin{bmatrix} \sigma_{A'A'} & \sigma_{A'B'} & \sigma_{A'C} \\ \sigma_{A'B'}^T & \sigma_{B'B'} & \sigma_{B'C} \\ \sigma_{A'C}^T & \sigma_{B'C}^T & \sigma_{CC} \end{bmatrix}, \quad (9)$$

四个模式的协方差矩阵为

$$\sigma_{nm} = \begin{bmatrix} \sigma_{A'A'} & \sigma_{A'B'} & \sigma_{A'C} & \sigma_{A'D} \\ \sigma_{A'B'}^T & \sigma_{B'B'} & \sigma_{B'C} & \sigma_{B'D} \\ \sigma_{A'C}^T & \sigma_{B'C}^T & \sigma_{CC} & \sigma_{CD} \\ \sigma_{A'D}^T & \sigma_{B'D}^T & \sigma_{CD}^T & \sigma_{DD} \end{bmatrix}. \quad (10)$$

以上协方差矩阵均可通过将(4)式带入其子矩阵的矩阵元获得。基于量子态的协方差矩阵，一个两组分($n_A + m_B$)系统 A 对 B 的导引特性可表征^[37]为

$$\mathcal{G}^{A \rightarrow B}(\sigma_{AB}) = \max \left\{ 0, - \sum_{j: \nu_j^{(AB\backslash A)} < 1} \ln [\nu_j^{(AB\backslash A)}] \right\}, \quad (11)$$

式中： v_j^{ABVA} ($j = 1, \dots, m_B$) 表示 $\bar{\sigma}_{ABVA}$ 的辛本征值^[38]，即 $|i\Omega \bar{\sigma}_{ABVA}|$ 。其中， $\bar{\sigma}_{ABVA} = \mathbf{B} - \mathbf{C}^T \mathbf{A}^{-1} \mathbf{C}$ 是 \mathbf{A} 的舒尔补码， $\Omega = \oplus_1^{n+m} \begin{bmatrix} 0 & 1 \\ -1 & 0 \end{bmatrix}$ ， \oplus_1^{n+m} 为一种辛形式，与两组分 ($n_A + m_B$) 系统相对应。在求得协方差矩阵后便可代入(11)式，得到两组分间的导引参数。 $\mathcal{G}^{A \rightarrow B}(\sigma_{AB}) = 0$ 表示系统 A 对 B 无导引能力， $\mathcal{G}^{A \rightarrow B}(\sigma_{AB}) > 0$ 表示系统 A 可以导引系统 B 。

同样，系统 B 对 A 的导引特性可以通过交换 A 和 B 获得：

$$\mathcal{G}^{B \rightarrow A}(\sigma_{AB}) = \max \left\{ 0, - \sum_{j: v_j^{(ABVA)} < 1} \ln [v_j^{(ABVA)}] \right\}. \tag{12}$$

当 $\mathcal{G}^{A \rightarrow B}(\sigma_{AB}) > 0$ 且 $\mathcal{G}^{B \rightarrow A}(\sigma_{AB}) = 0$ 或者 $\mathcal{G}^{A \rightarrow B}(\sigma_{AB}) = 0$ 且 $\mathcal{G}^{B \rightarrow A}(\sigma_{AB}) > 0$ 时，系统 A 与 B 之间为单方向的 EPR 导引。

3 结果分析

图 2 是 \hat{A}' 和 \hat{B}' 间导引参数随着高斯噪声和分束器透射率 η 的导引变化关系，输入模的压缩参数为 0.69，相当于 6 dB 的压缩。图 2(a) 是透射率为 0.9 时， \hat{A}' 和 \hat{B}' 间导引参数随着高斯噪声的变化关系，实线表示 \hat{A}' 对 \hat{B}' 的导引，虚线表示 \hat{B}' 对 \hat{A}' 的导引。可以看出： \hat{A}' 和 \hat{B}' 间为双向导引时高斯噪声为 $(0, 0.05]$ ； \hat{B}' 对 \hat{A}' 单向导引时高斯噪声为 $(0.05, 0.18]$ ；当高斯噪声大于 0.18 时， \hat{A}' 和 \hat{B}' 间无导引。图 2(b) 为不同高斯噪声下的 \hat{A}' 和 \hat{B}' 间的导引参数随分束器透射率 η 的变化关系，实线表示 \hat{A}' 对 \hat{B}' 的导引，虚线表示 \hat{B}' 对 \hat{A}' 的导引。可以看出：当无高斯噪声时， \hat{B}' 对 \hat{A}' 单向导引范围为 $0.22 \leq \eta \leq 0.83$ ；当高斯噪声为 0.03 时， \hat{B}' 对 \hat{A}' 单向导引范围

为 $0.31 \leq \eta \leq 0.87$ ；当高斯噪声为 0.06 时， \hat{B}' 对 \hat{A}' 单向导引范围为 $0.42 \leq \eta \leq 0.91$ 。这表明通过调节有损信道中的透射率以及加入不同的高斯噪声，可以在大范围内实现两个模式间的单方向 EPR 导引操控。

图 3 为 $(1+2)$ 模式和 $(2+1)$ 模式下的 EPR 导引图，输入模的压缩参数为 0.69。图 3(a)、(b) 是 \hat{A}' 和 $\hat{B}'\hat{C}$ 间的导引情况。图 3(a) 是 \hat{A}' 和 $\hat{B}'\hat{C}$ 间的导引参数随高斯噪声的变化关系图，实线表示 \hat{A}' 对 $\hat{B}'\hat{C}$ 的导引，虚线表示 $\hat{B}'\hat{C}$ 对 \hat{A}' 的导引。当高斯噪声为 $[0, 0.489]$ 时， \hat{A}' 和 $\hat{B}'\hat{C}$ 间的导引是双向的。当高斯噪声为 $(0.489, 1)$ 时， \hat{A}' 和 $\hat{B}'\hat{C}$ 间是 $\hat{B}'\hat{C}$ 对 \hat{A}' 的单向导引。图 3(b) 是高斯噪声为 $[0, 0.489]$ 内三个不同值时， \hat{A}' 和 $\hat{B}'\hat{C}$ 间的导引参数随透射率 η 的变化关系图，实线表示 \hat{A}' 对 $\hat{B}'\hat{C}$ 的导引，虚线表示 $\hat{B}'\hat{C}$ 对 \hat{A}' 的导引。可以发现，随着透射率 η 的变化，当高斯噪声取值增大时， $\hat{B}'\hat{C}$ 对 \hat{A}' 的单向导引范围也在增大。同样地，图 3(c)、(d) 是 \hat{B}' 和 $\hat{A}'\hat{C}$ 间导引参数的变化关系图，可以发现，通过加入高斯噪声以及调节有损信道中的透射率，可以在大范围内实现 \hat{B}' 和 $\hat{A}'\hat{C}$ 间的单向导引操控。

图 4 为 $(1+3)$ 模式和 $(3+1)$ 模式下的 EPR 导引关系图，输入模的压缩参数为 0.69。图 4(a) 是 \hat{A}' 和 $\hat{B}'\hat{C}\hat{D}$ 间的导引参数随高斯噪声的变化关系图，实线表示 \hat{A}' 对 $\hat{B}'\hat{C}\hat{D}$ 的导引，虚线表示 $\hat{B}'\hat{C}\hat{D}$ 对 \hat{A}' 的导引。当高斯噪声为 $[0, 2]$ 时，无法实现 \hat{A}' 和 $\hat{B}'\hat{C}\hat{D}$ 间的单向导引。图 4(b) 是 \hat{A}' 和 $\hat{B}'\hat{C}\hat{D}$ 间的导引参数随透射率 η 的变化关系图，实线表示 \hat{A}' 对 $\hat{B}'\hat{C}\hat{D}$ 导引，虚线 $\hat{B}'\hat{C}\hat{D}$ 对 \hat{A}' 的导引。当高斯噪声为 0 时， $\hat{B}'\hat{C}\hat{D}$ 对 \hat{A}' 的单向导引范围是 $0 < \eta < 0.498$ 。当高斯噪声为 0.5 时， $\hat{B}'\hat{C}\hat{D}$ 对 \hat{A}' 的单向

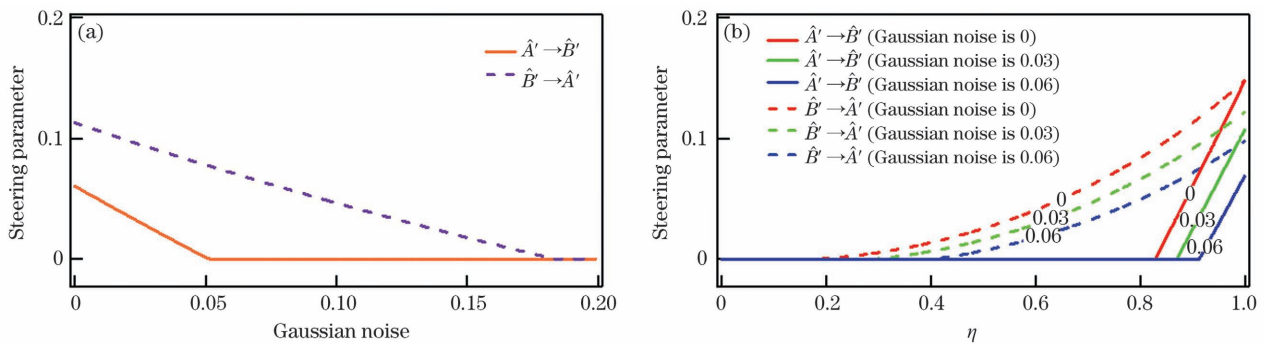


图 2 \hat{A}' 和 \hat{B}' 间的 EPR 导引。(a) 当 $\eta = 0.9$ 时， \hat{A}' 和 \hat{B}' 间 EPR 导引参数随高斯噪声的变化关系；(b) \hat{A}' 和 \hat{B}' 间 EPR 导引参数随透射率的变化关系

Fig. 2 EPR steering between \hat{A}' and \hat{B}' . (a) EPR steering parameter versus Gaussian noise between \hat{A}' and \hat{B}' when $\eta = 0.9$; (b) EPR steering parameter versus transmissivity between \hat{A}' and \hat{B}'

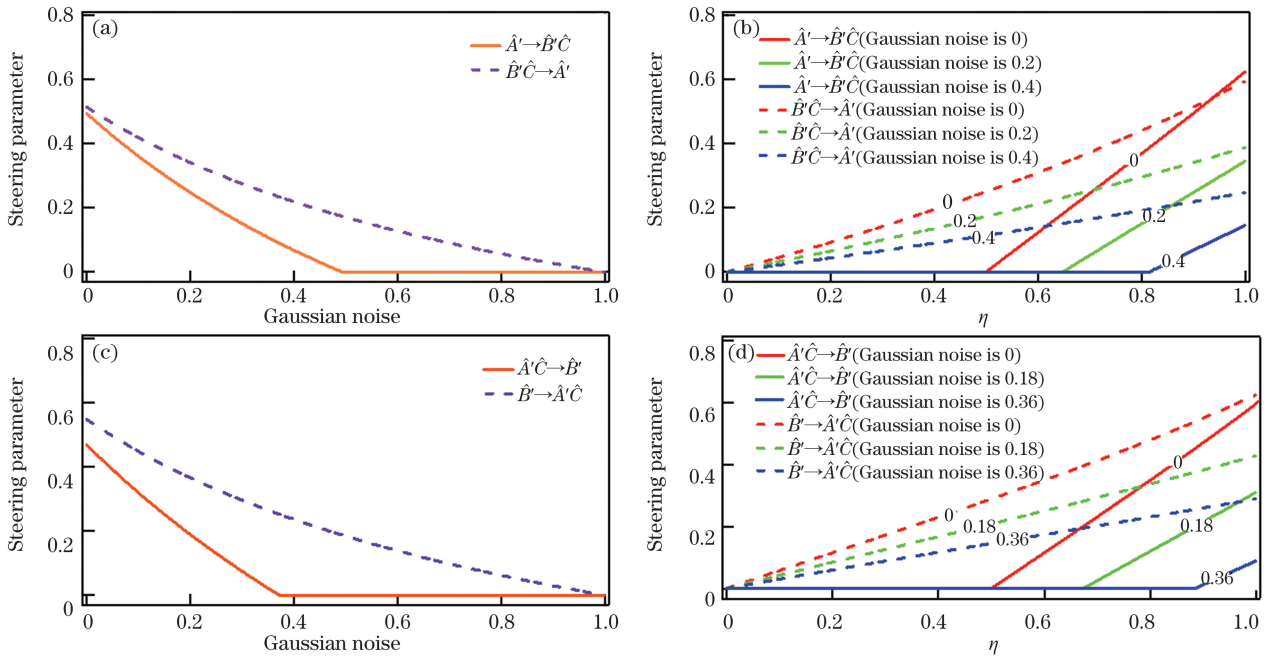


图 3 (1+2)模式和(2+1)模式下的 EPR 导引。(a)当 $\eta=0.9$ 时, \hat{A}' 和 $B'\hat{C}$ 间 EPR 导引参数随高斯噪声的变化关系; (b) \hat{A}' 和 $B'\hat{C}$ 间 EPR 导引参数随透射率的变化关系; (c)当 $\eta=0.9$ 时, \hat{B}' 和 $\hat{A}'\hat{C}$ 间 EPR 导引参数随高斯噪声的变化关系; (d) \hat{B}' 和 $\hat{A}'\hat{C}$ 间 EPR 导引参数随透射率的变化关系

Fig. 3 EPR steering in (1+2) mode and (2+1) mode. (a) EPR steering parameter versus Gaussian noise δ between \hat{A}' and $B'\hat{C}$ when $\eta=0.9$; (b) EPR steering parameter versus transmissivity between \hat{A}' and $B'\hat{C}$; (c) EPR steering parameter versus Gaussian noise between \hat{B}' and $\hat{A}'\hat{C}$ when $\eta=0.9$. (d) EPR steering parameter versus transmissivity between \hat{B}' and $\hat{A}'\hat{C}$

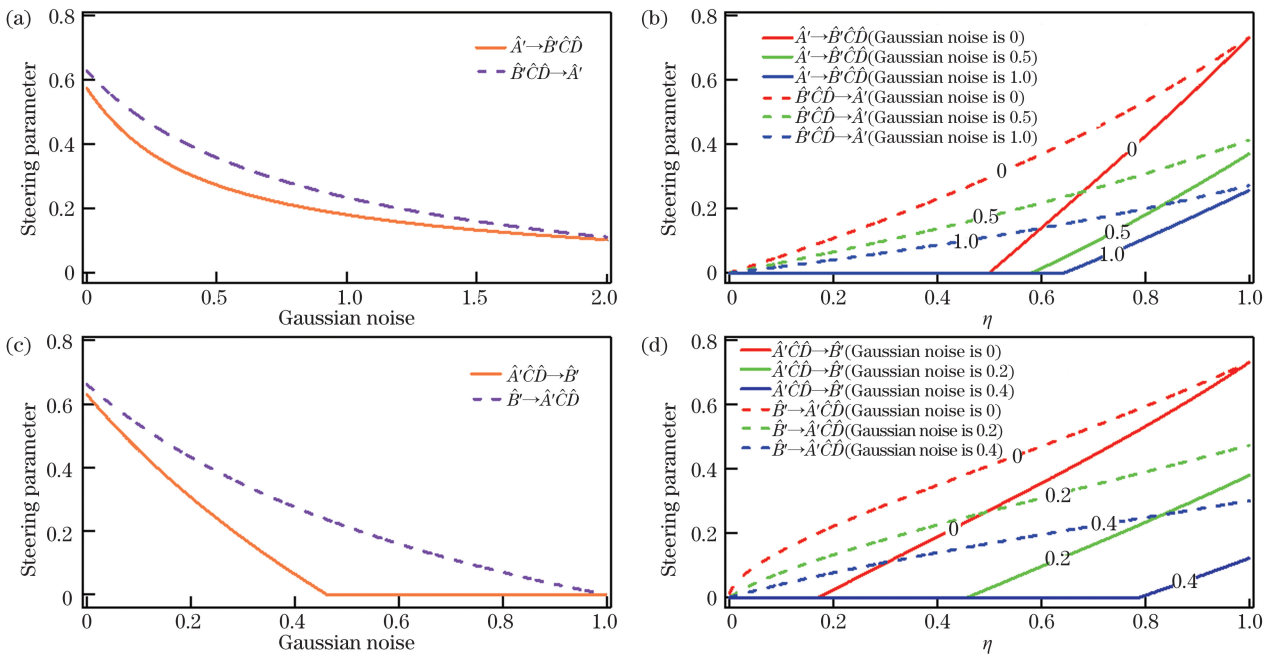


图 4 (1+3)模式和(3+1)模式下的 EPR 导引。(a)当 $\eta=0.9$ 时, \hat{A}' 和 $B'\hat{C}\hat{D}$ 间 EPR 导引参数随高斯噪声的变化关系; (b) \hat{A}' 和 $B'\hat{C}\hat{D}$ 间 EPR 导引参数随透射率的变化关系; (c)当 $\eta=0.9$ 时, \hat{B}' 和 $\hat{A}'\hat{C}\hat{D}$ 间 EPR 导引参数随高斯噪声的变化关系; (d) \hat{B}' 和 $\hat{A}'\hat{C}\hat{D}$ 间 EPR 导引参数随透射率的变化关系

Fig. 4 EPR steering in (1+3) mode and (3+1) mode. (a) EPR steering parameter versus Gaussian noise between \hat{A}' and $B'\hat{C}\hat{D}$ when $\eta=0.9$; (b) EPR steering parameter versus transmissivity between \hat{A}' and $B'\hat{C}\hat{D}$; (c) EPR steering parameter versus Gaussian noise between \hat{B}' and $\hat{A}'\hat{C}\hat{D}$ when $\eta=0.9$; (d) EPR steering parameter versus transmissivity between \hat{B}' and $\hat{A}'\hat{C}\hat{D}$

导引范围是 $0 < \eta < 0.586$ 。当高斯噪声为 1.0 时, $\hat{B}'\hat{C}\hat{D}$ 对 \hat{A}' 的单向导引范围是 $0 < \eta < 0.640$ 。图 4(c) 是当透射率 $\eta = 0.9$ 时, \hat{B}' 和 $\hat{A}'\hat{C}\hat{D}$ 间的导引参数随高斯噪声的变化关系图。可以看出: 当 \hat{B}' 和 $\hat{A}'\hat{C}\hat{D}$ 间为双向导引时, 高斯噪声为 $[0, 0.436]$; 当 \hat{B}' 对 $\hat{A}'\hat{C}\hat{D}$ 单向导引时, 高斯噪声为 $[0.436, 0.970]$ 。图 4(d) 是高斯噪声为 $[0, 0.436]$ 内三个不同值时, \hat{B}' 和 $\hat{A}'\hat{C}\hat{D}$ 间的导引参数随透射率 η 的变化关系图。可以看出, 随着透射率 η 的变化, 所加高斯噪声值越大, \hat{B}' 对 $\hat{A}'\hat{C}\hat{D}$ 的单向导引范围就越大。因此, 通过调节有损信道中的透射率以及加入合适的噪声, 可以在大范围内实现 (1+3) 模式和 (3+1) 模式的单向 EPR 导引操控。

图 5 是 (2+2) 模式下的 EPR 导引, 输入模的

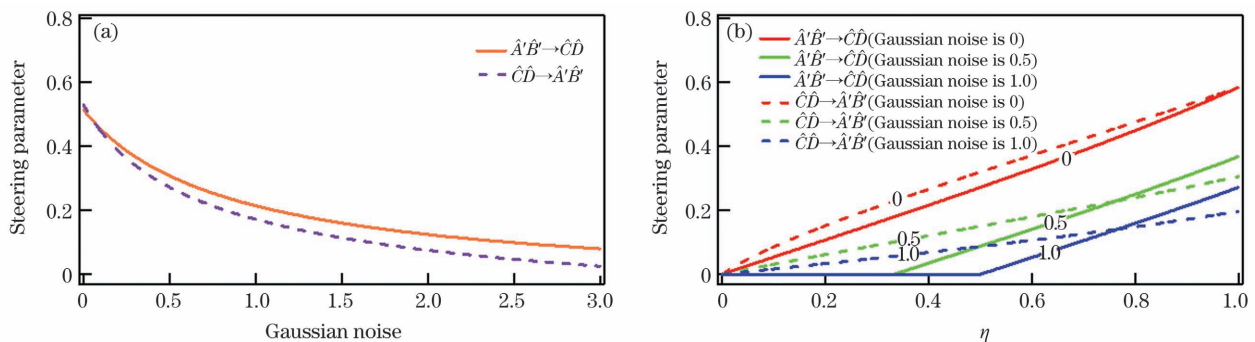


图 5 (2+2) 模式下的 EPR 导引。(a) 当 $\eta = 0.9$ 时, $\hat{A}'\hat{B}'$ 和 $\hat{C}\hat{D}$ 间 EPR 导引参数随高斯噪声的变化关系; (b) $\hat{A}'\hat{B}'$ 和 $\hat{C}\hat{D}$ 间 EPR 导引参数随透射率的变化关系

Fig. 5 EPR steering in (2+2) mode. (a) EPR steering parameter versus Gaussian noise between $\hat{A}'\hat{B}'$ and $\hat{C}\hat{D}$ when $\eta = 0.9$; (b) EPR steering parameter versus transmissivity between $\hat{A}'\hat{B}'$ and $\hat{C}\hat{D}$

4 结 论

基于四组分方形 Cluster 态, 通过加入高斯噪声以及调节分束器引入的有损信道中的透射率, 实现了不同模式间的单向 EPR 导引。研究表明, 与未加入噪声和调节透射率的情况相比, 同时加入噪声和调节透射率, 不同模式间的单向导引操控更易实现, 操控范围也更广。所提方案操作简单, 易于实现, 可满足不同用户间信息安全传递的要求, 如单端设备无关量子密钥分发以及量子秘密共享。此外, 结合当前量子通信的发展, 所研究的单向量子导引对远距离传输的量子安全通信也有一定参考价值。

参 考 文 献

- [1] Einstein A, Podolsky B, Rosen N. Can quantum-mechanical description of physical reality be considered complete? [J]. Physical Review, 1935, 47 (10): 777-780.
- [2] Schrödinger E. Discussion of probability relations between separated systems [J]. Mathematical Proceedings of the Cambridge Philosophical Society, 1935, 31(4): 555-563.
- [3] Wiseman H M, Jones S J, Doherty A C. Steering, entanglement, nonlocality, and the Einstein-Podolsky-Rosen paradox [J]. Physical Review Letters, 2007, 98(14): 140402.
- [4] Branciard C, Cavalcanti E G, Walborn S P, et al. One-sided device-independent quantum key distribution: security, feasibility, and the connection with steering [J]. Physical Review A, 2012, 85(1): 010301.
- [5] Gehring T, Händchen V, Dühme J, et al. Implementation of continuous-variable quantum key distribution with composable and one-sided-device-independent security against coherent attacks [J]. Nature Communications, 2015, 6: 8795.
- [6] He Y F, Li C Y, Guo J R, et al. Passive measurement-

- device-independent quantum key distribution based on heralded pair coherent states [J]. *Chinese Journal of Lasers*, 2020, 47(9): 0912002.
- 何业锋, 李春雨, 郭佳瑞, 等. 基于标记配对相干态的被动测量设备无关量子密钥分配 [J]. *中国激光*, 2020, 47(9): 0912002.
- [7] He Y F, Zhao Y K, Li C Y, et al. Measurement-device-independent quantum key distribution of finite detector's dead time in heralded pair coherent state [J]. *Acta Optica Sinica*, 2020, 40(24): 2427001.
- 何业锋, 赵艳坤, 李春雨, 等. 标记配对相干态下有限探测器死时间的测量设备无关量子密钥分配 [J]. *光学学报*, 2020, 40(24): 2427001.
- [8] Xiang Y, Su X L, Mišta L, et al. Multipartite Einstein-Podolsky-Rosen steering sharing with separable states [J]. *Physical Review A*, 2019, 99(1): 010104.
- [9] Reid M D. Signifying quantum benchmarks for qubit teleportation and secure quantum communication using Einstein-Podolsky-Rosen steering inequalities [J]. *Physical Review A*, 2013, 88(6): 062338.
- [10] He Q Y, Rosales-Zárate L, Adesso G, et al. Secure continuous variable teleportation and Einstein-Podolsky-Rosen steering [J]. *Physical Review Letters*, 2015, 115(18): 180502.
- [11] Jones S J, Wiseman H M, Doherty A C. Entanglement, Einstein-Podolsky-Rosen correlations, Bell nonlocality, and steering [J]. *Physical Review A*, 2007, 76(5): 052116.
- [12] Briegel H J, Dür W, Cirac J I, et al. Quantum repeaters: the role of imperfect local operations in quantum communication [J]. *Physical Review Letters*, 1998, 81(26): 5932-5935.
- [13] Duan L M, Monroe C. Colloquium: quantum networks with trapped ions [J]. *Reviews of Modern Physics*, 2010, 82(2): 1209-1224.
- [14] Duan L M, Lukin M D, Cirac J I, et al. Long-distance quantum communication with atomic ensembles and linear optics [J]. *Nature*, 2001, 414(6862): 413-418.
- [15] Händchen V, Eberle T, Steinlechner S, et al. Observation of one-way Einstein-Podolsky-Rosen steering [J]. *Nature Photonics*, 2012, 6(9): 596-599.
- [16] He Q Y, Reid M D. Genuine multipartite Einstein-Podolsky-Rosen steering [J]. *Physical Review Letters*, 2013, 111(25): 250403.
- [17] Armstrong S, Wang M, Teh R Y, et al. Multipartite Einstein-Podolsky-Rosen steering and genuine tripartite entanglement with optical networks [J]. *Nature Physics*, 2015, 11(2): 167-172.
- [18] Qin Z Z, Deng X W, Tian C X, et al. Manipulating the direction of Einstein-Podolsky-Rosen steering [J]. *Physical Review A*, 2017, 95(5): 052114.
- [19] Walther P, Resch K J, Rudolph T, et al. Experimental one-way quantum computing [J]. *Nature*, 2005, 434(7030): 169-176.
- [20] Su X L, Hao S H, Deng X W, et al. Gate sequence for continuous variable one-way quantum computation [J]. *Nature Communications*, 2013, 4: 2828.
- [21] Bowles J, Vértesi T, Quintino M T, et al. One-way Einstein-Podolsky-Rosen steering [J]. *Physical Review Letters*, 2014, 112(20): 200402.
- [22] Skrzypczyk P, Navascués M, Cavalcanti D. Quantifying Einstein-Podolsky-Rosen steering [J]. *Physical Review Letters*, 2014, 112(18): 180404.
- [23] Sun K, Ye X J, Xu J S, et al. Experimental quantification of asymmetric Einstein-Podolsky-Rosen steering [J]. *Physical Review Letters*, 2016, 116(16): 160404.
- [24] Zhang J, Braunstein S L. Continuous-variable Gaussian analog of cluster states [J]. *Physical Review A*, 2006, 73(3): 032318.
- [25] van Loock P, Weedbrook C, Gu M L. Building Gaussian Cluster states by linear optics [J]. *Physical Review A*, 2007, 76(3): 032321.
- [26] Lu C Y, Yang T, Pan J W. Experimental multiparticle entanglement swapping for quantum networking [J]. *Physical Review Letters*, 2009, 103(2): 020501.
- [27] van Loock P, Braunstein S L. Multipartite entanglement for continuous variables: a quantum teleportation network [J]. *Physical Review Letters*, 2000, 84(15): 3482-3485.
- [28] van Loock P, Braunstein S L. Greenberger-Horne-Zeilinger nonlocality in phase space [J]. *Physical Review A*, 2001, 63(2): 022106.
- [29] Muralidharan S, Panigrahi P K. Quantum-information splitting using multipartite cluster states [J]. *Physical Review A*, 2008, 78(6): 1-5.
- [30] Lau H K, Weedbrook C. Quantum secret sharing with continuous-variable cluster states [J]. *Physical Review A*, 2013, 88(4): 042313.
- [31] Deng X W, Xiang Y, Tian C X, et al. Demonstration of monogamy relations for Einstein-Podolsky-Rosen steering in Gaussian Cluster states [J]. *Physical Review Letters*, 2017, 118(23): 230501.
- [32] Zhai S Q, Yuan N, Liu K. Asymmetric Einstein-Podolsky-Rosen steering manipulating among multipartite entangled states [J]. *Journal of the Optical Society of America B*, 2019, 36(10): 2920-2926.
- [33] Zhai S Q, Yuan N, Li Q. Asymmetric bipartite EPR

- steering swapping characteristics of continuous variable [J]. *Acta Optica Sinica*, 2020, 40(4): 0427001.
- 翟淑琴, 袁楠, 李倩. 连续变量两组分非对称 EPR 导引交换特性 [J]. *光学学报*, 2020, 40(4): 0427001.
- [34] Kogias I, Xiang Y, He Q Y, et al. Unconditional security of entanglement-based continuous-variable quantum secret sharing [J]. *Physical Review A*, 2017, 95: 012315.
- [35] van Loock P, Furusawa A. Detecting genuine multipartite continuous-variable entanglement [J]. *Physical Review A*, 2003, 67(5): 052315.
- [36] Adesso G, Illuminati F. Entanglement in continuous-variable systems: recent advances and current perspectives [J]. *Journal of Physics A*, 2007, 40(28): 7821-7880.
- [37] Kogias I, Lee A R, Ragy S, et al. Quantification of Gaussian quantum steering [J]. *Physical Review Letters*, 2015, 114(6): 060403.
- [38] Serafini A. Multimode uncertainty relations and separability of continuous variable states [J]. *Physical Review Letters*, 2006, 96(11): 110402.

Manipulated Multipartite Continue-Variable EPR Steering with Loss and Gaussian Noise

Zhai Shuqin^{1,2*}, Yuan Nan¹

¹ College of Physics and Electronic Engineering, Shanxi University, Taiyuan, Shanxi 030006, China;

² State Key Laboratory of Quantum Optics and Quantum Optics Devices, Institute of Opto-Electronics, Shanxi University, Taiyuan, Shanxi 030006, China

Abstract

Objective EPR steering is a quantum correlation between quantum entanglement and Bell nonlocality. Multipartite EPR steering, which manipulates information distributed in distinct quantum nodes, is a core resource in secret quantum networks. EPR steering describes a phenomenon in which two particles in the entangled state, Alice and Bob, are spread to distant places. Bob can be steered to a certain eigenvalue quantum state through the measurement of Alice, and Alice can be steered to a certain eigenvalue quantum state through the measurement of Bob. Situations in which Alice can steer Bob's state but Bob cannot steer Alice's state, or Bob can steer Alice's state but Alice cannot steer's Bob state, are referred as one-way EPR steering. EPR steering has been widely used in one-way quantum communication, such as one-sided device-independent quantum secret key distribution, secure quantum teleportation, and secure quantum networks, due to its unique asymmetric character. The entanglement persistence of continuous variable (CV) Cluster quantum entangled states is better than GHZ states. Many quantum communication operations based on Cluster states have been demonstrated due to their advantages, and the CV Cluster states quantum steering and its applications are exciting. Multipartite EPR steering is demonstrated in this study using a lossy channel in one mode of a quadripartite entanglement state and adding Gaussian noise in another. This study will be useful for advancing quantum information science and provide a reliable guarantee for the one-way requirements of secure quantum communication operations such as quantum teleportation and quantum secret sharing.

Methods The schematic of the physical system for manipulating the direction of EPR steering with loss and Gaussian noise is shown in Fig. 1. As shown in this figure, two phase-squeezed optical modes and two amplitude-squeezed optical modes are used as input modes, and they pass through three beam splitters to yield four entangled output modes. The four output modes are described by $\hat{A}, \hat{B}, \hat{C}, \hat{D}$. Multipartite EPR steering is demonstrated by introducing a lossy channel in one mode of the quadripartite entangled states and adding Gaussian noise in another mode. Here we consider a lossy quantum channel in mode \hat{A} , and after introducing loss, mode \hat{A} is converted into mode \hat{A}' . We introduces a Gaussian noise in mode \hat{B} by a 99:1 beam splitter, and \hat{B} is converted into \hat{B}' subsequently. The final modes $\hat{A}', \hat{B}', \hat{C}, \hat{D}$ are correlated with each other. First, the covariance matrices of the different combinations of multipartite states are reconstructed, then the manipulated quantum steering in bipartite, tripartite, and quadripartite are investigated. The EPR steering parameter versus Gaussian noise is obtained, and in

the same way, EPR steering characteristic versus transmissivity in the lossy channel is analyzed. After that, the steering images are compared and analyzed to verify one-way EPR steering.

Results and Discussions The changes of EPR steering parameters between different modes with Gaussian noise and transmissivity are analyzed. Fig. 2 shows the steering direction manipulation of (1 + 1) mode. Fig. 2(a) shows that a one-way EPR steering range varies with Gaussian noise when the transmissivity is settled. Fig. 2(b) shows that EPR steering parameter varies with the transmissivity when Gaussian noise is settled. This shows one-way steering, and two-way steering between \hat{A}' and \hat{B}' can be obtained when different Gaussian noise is added. Fig. 3 shows the EPR steering in (1 + 2) mode and (2 + 1) mode of the Cluster states. Fig. 4 shows the EPR steering in (1 + 3) mode and (3 + 1) mode of the Cluster state. Finally, we analyze EPR steering parameters between two collaboration modes as shown in Fig. 5. Thus, we can achieve different types of EPR steering in a larger range by adjusting the transmissivity of a lossy channel and adding Gaussian noise.

Conclusions This study investigates EPR steering among various combinations using quadripartite Cluster entangled states, by introducing loss and Gaussian noise in different modes. When the light modes are distributed in the quantum network, the manipulation effects of the lossy channel and Gaussian noise on the EPR steering are examined. The EPR quantum steering distributed in bipartite, tripartite, and quadripartite is discussed. The theoretical study confirms that the one-way EPR steering manipulation can be realized more easily and widely by adding the lossy channel and Gaussian noise. Gaussian one-way quantum steering directly enriches the one-sided device-independent quantum key distribution and quantum secret sharing schemes. The application of one-way quantum steering, which we study in long-distance secure quantum communication, is also crucial when combined with current quantum communication needs.

Key words quantum optics; EPR steering; one-way steering; asymmetry; noise; quantum networks

OCIS codes 270.2500; 270.5565; 270.5585; 270.6570